

Lost in Projection? Gaussian Filtering Recovers Hidden Conformational States

Sofia Sartore, Daniel Nagel, Georg Diez, and Gerhard Stock*

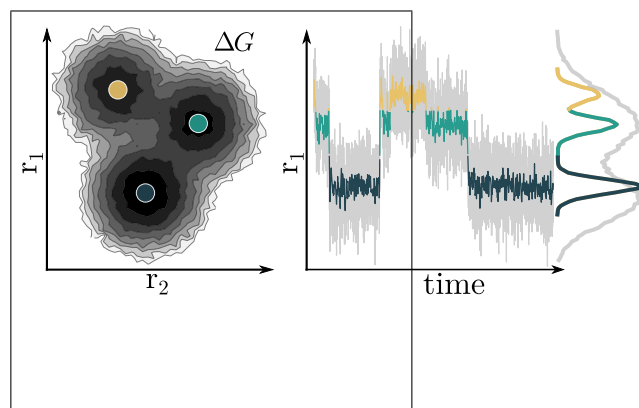
Biomolecular Dynamics, Institute of Physics, University of Freiburg, 79104 Freiburg, Germany

E-mail: stock@physik.uni-freiburg.de

Abstract

To interpret molecular dynamics (MD) simulations, it is common practice to reduce the dimensionality of the molecular coordinates to a low-dimensional collective variable x . Projecting the high-dimensional MD data onto x yields a free energy landscape $\Delta G(x)$, which highlights low-energy regions corresponding to conformational states. The accurate definition of these states, however, is often impeded by projection artifacts, resulting in artificially shortened state lifetimes or even the complete disappearance of states from the analysis. As demonstrated for a two-dimensional toy model, Gaussian low-pass filtering of the high-dimensional MD coordinates can restore the underlying free energy landscape, allowing to recover previously hidden states. When applied to an all-atom folding trajectory of HP35, the number of microstates increases by an order of magnitude, which leads to metastable states that are long-lived and much better defined structurally, even compared to dynamically cored state trajectories.

TOC Graphic



Complex dynamical systems, like solvated proteins, are characterized by dynamics that span multiple timescales. The output of molecular dynamics (MD) simulations provides the time evolution of the atomic coordinates, capturing fast local fluctuations and slower global conformational rearrangements.¹ Since the latter usually constitute the processes of interest, the analysis of MD simulations involves separating fast and slow motions. This is often done by identifying metastable conformational states and modeling the dynamics of interest by a series of memoryless transitions between these states, yielding a Markov state model (MSM).^{2–7} This approach is widely used, since it holds the promise of predicting long-term dynamics from short trajectories, and because its use is facilitated by workflow implementations in software packages like PyEmma,⁸ MSMBuilder,⁹ and msmhelper.¹⁰

Building meaningful MSMs from MD data, however, presents the challenge of correctly identifying metastable states. The high-dimensional space of atomic coordinates compromises this task at the very start, because the sparsity of the data distribution hinders statistical robustness. This issue can in principle be overcome by the assumption that protein dynamics reside on low-dimensional manifolds.^{11,12} All dimensionality reduction techniques, from straightforward linear principal component analysis¹³ to sophisticated deep-learning autoencoder strategies^{14,15} exploit this manifold hypothesis in order to project the initial coordinates onto a low-dimensional space of collective variables and effectively capture essential dynamics. The reduced-dimensional energy landscape of such projected coordinates is then scanned with a clustering algorithm that identifies the minima corresponding to metastable states. Density-based methods^{16–19} are a valuable alternative to the widely used geometric clusterings (such as k -means²⁰) in MSM construction, as they perform better in defining states at the barriers.²¹ However, despite many advances in dimensionality reduction and clustering techniques, projecting high-dimensional data onto a lower-dimensional space often leads to misclassifications of data points, especially in sparsely populated transi-

tion regions. This hampers a proper definition of the states and their metastability, causing fast intrastate fluctuations to be interpreted as interstate transitions, which leads to an underestimation of the timescales of the processes under study. Even worse, it may also lead to the complete disappearance of states from the analysis.

A simple way of correcting these projection artifacts was introduced with the concept of coring.³ From a geometrical perspective, a core is defined as the region surrounding the center of a state. The idea is that the system should reach that region for a transition to a new state to be considered completed, thus resulting in a modified state trajectory.^{22,23} However, as the definition of geometrical cores is not always trivial, especially in the case of high dimensional coordinates, dynamical variants of coring were also introduced. These are generally based on the requirement that the system spends a minimum amount of time—the coring time t_{cor} —in the new state after transitioning.^{24,25} Hence, t_{cor} poses a limit for the time resolution on the interstate dynamics, and must therefore be chosen shorter than the fastest dynamics of interest.

Despite being effective in curing spurious interstate fluctuations, coring of the state trajectory cannot correct for the loss of states in the analysis, because coring is applied after the definition of states. This means that if the projection step causes the disappearance of free energy barriers (and thus the loss of states), coring of the state trajectory is not sufficient to recover the full dynamics. Recently, it has been shown that missing degrees of freedom can be recovered using time-aware representation learning methods exploiting temporal correlations.^{26,27} To introduce a data pre-processing step at the level of the input coordinates, in this work we discuss ‘Gaussian filtering’^{28,29} that mitigates projection artifacts before clustering, by eliminating the high-frequency fluctuations in the coordinates trajectory. Acting as a low-pass filter, it is shown to improve the accuracy of state identification and subsequent MSM construction. While the use of low-pass filtering has been suggested before in the field of Markov modeling,^{30–32} we believe that its impact, util-

ity, and consequences for MSM construction have not been fully appreciated so far.

We start with an intuitive example that reveals why artifacts are introduced by projecting data on a lower dimension and how the above-mentioned corrective approaches can offer promising solutions. The model consists of three potential wells separated by barriers of similar height ($\sim 4 k_B T$), see Fig. 1. For this simple toy model, it is straightforward to define a true (i.e., optimal) reaction coordinate, s , following the lines connecting the minima,³³ i.e., the segment between wells 1 and 2 for $x \leq 0$, and the one between wells 2 and 3 for $x > 0$. We then run an overdamped Langevin simulation to sample the corresponding 2D free energy landscape (Fig. 1a). As shown by the resulting 1D free energy curve $\Delta G(s)$ in Fig. 1b, the three minima are clearly separated along s . The frames can be readily assigned to three states by cutting the curve exactly at the barriers, whose height is preserved from the 2D case. Figure 1c shows an example of the time trace of s , where the color of each frame represents the state it is assigned to. All three states are recovered and clearly separated, because along the true reaction coordinate the overdamped Langevin trajectory exhibits no immediate recrossing of the barrier after a transition, as it proceeds to the minimum of the new state. As a consequence, the state trajectories obtained from the 2D energy landscape $\Delta G(x, y)$ and the 1D landscape $\Delta G(s)$ are equivalent.

The situation becomes more involved in the—more realistic—case in which we only have a suboptimal reaction coordinate. To mimic this and illustrate how projection artifacts can arise in our toy model, we use s as a reference and define in Fig. 1a two additional 1D reaction coordinates, where the projection effects become progressively worse: the projection on the x -axis $\mathbf{x} = x \mathbf{e}_x$, and the projection on the tilted axis $\mathbf{r} = r \mathbf{e}_r$.

As shown in Fig. 2a, the three minima of $\Delta G(x)$ are still clearly distinguishable, but the barriers between them become smaller ($\sim 1 k_B T$) than in the original 2D landscape. Moreover, the time trace of x (Fig. 2b) shows ‘overshooting’ at the barrier between states: tran-

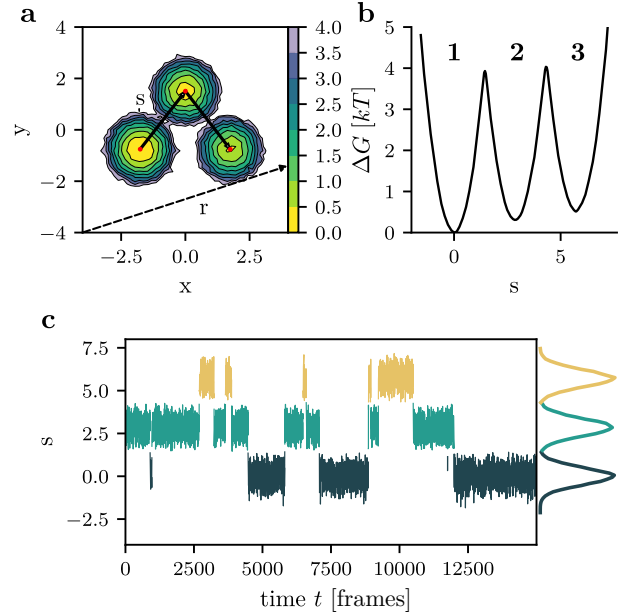


Figure 1: Three-well model. (a) 2D free energy landscape $\Delta G(x, y)$ as a function of the original coordinates x and y . Indicated are the optimal 1D coordinate, s , directly connecting the three minima, and a suboptimal coordinate, r , obtained via the projection on vector \mathbf{r} . (b) Projection of the 2D data on the optimal reaction coordinate s yields the barrier-preserving free energy curve $\Delta G(s)$. (c) Trajectory of the optimal reaction coordinate, color coded by the state that each frame is assigned to.

sient fluctuations that are wrongly identified as transitions between states can be easily spotted as two different colors alternating very rapidly. This happens because frames located at the barriers of $\Delta G(x)$ may already belong to the adjacent state in the orthogonal y -direction. The loss of this information can be seen from the definition of the 1D free energy as

$$\Delta G(x) = -k_B T \ln P(x) \quad (1)$$

with

$$P(x) = \int dy P(x, y). \quad (2)$$

When we consider the 2D probability distribution $P(x_{12}, y)$ at the barrier between states 1 and 2 along x (on the side of state 1), clearly the system may be already in state 2 along the y coordinate. As a result, the 1D trajectory $x(t)$ exhibits the typical projection artifact of

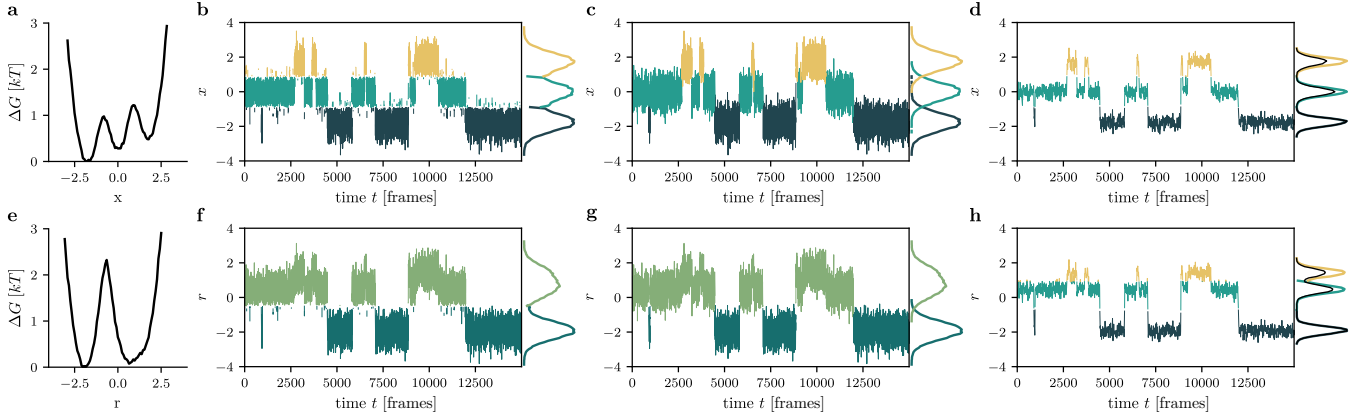


Figure 2: Effects of suboptimal 1D reaction coordinates x (top) and r (bottom) chosen for the 2D model. Shown are (left) 1D energy curves and (right) color-coded time traces with states assigned by cutting at the barrier. Panels (b, f) shows the raw data, (c, g) the results after applying iterative coring ($t_{\text{cor}} = 10$ frames), and (d, h) the results after applying Gaussian filtering ($t_{\text{GF}} = 10$ frames). The right side of each panel shows the respective state-resolved distributions.

appearing to fluctuate rapidly back and forth across the barrier.

As a remedy, we apply dynamical coring,^{24,25} e.g., we request that the trajectory stays at least $t_{\text{cor}} = 10$ frames in the new state. As shown in Fig. 2c, this simple measure already eliminates most of the spurious transitions at the barriers. In this way, the coring effectively reduces the overlap of the states' probability distributions in the border regions. Since already small fluctuations may mask true transitions, it is in fact advantageous to iteratively core the state trajectory,³⁴ by using coring times incrementing from $t_{\text{cor}} = 2$ to 10 frames, rather than performing a single coring process with $t_{\text{cor}} = 10$ frames. Iterative coring is found to reduce the number of reassigned MD frames i.e., it changes the original trajectory less, while still smoothing with the same time resolution.³⁵

Alternatively, we may apply a Gaussian filter function with standard deviation σ on the feature trajectory $x(t)$,^{28,29}

$$x(t) \rightarrow \sum_j \frac{1}{\sqrt{2\pi\sigma^2}} \exp\left[-\frac{(t_j - t)^2}{2\sigma^2}\right] x(t_j). \quad (3)$$

It affects a smoothing of $x(t)$ within a moving window of approximately $t_{\text{GF}} = 2\sigma$, corresponding to a low-pass filter with a cut-off frequency $1/t_{\text{GF}}$. Using $t_{\text{GF}} = 10$ frames, Fig. 2d reveals that this smoothing results in a clear

separation of the three energy basins. This is because Gaussian filtering causes a reduction of the amplitude of the fluctuations, which results in a narrowing of the distance distributions of the states. Hence we achieve a better resolved structure of the free energy landscape with clearly defined barriers, before assigning the time series to states.

In the second, more drastic, case, we choose $\mathbf{r} = r \mathbf{e}_r$ (see Fig. 1a) as projection axis for our model. The resulting free energy $\Delta G(r)$ (Fig. 2e) reveals that one barrier is lost and only two states can be distinguished. Figure 2g shows the time-trace $r(t)$ after applying iterative dynamical coring ($t_{\text{cor}} = 10$ frames) on the state trajectory. While the coring eliminates the fast fluctuations between the two states, it obviously cannot recover the information that is missing in the free energy landscape $\Delta G(r)$, as it can only reassign frames among the two states that were already identified. Nonetheless, the time evolution of $r(t)$ still suggests the existence of three states (Fig. 2f), hence the question is how to retrieve this information at the level of the free energy.

Here the advantage of curing the problem at the level of the input coordinates is even more obvious, as can be seen in Fig. 2h. By applying Gaussian filtering to $r(t)$ with a short window of $t_{\text{GF}} = 10$ frames, the reduced fluctuations of $r(t)$ facilitate the identification of all three minima of the free energy $\Delta G(r)$, and therefore

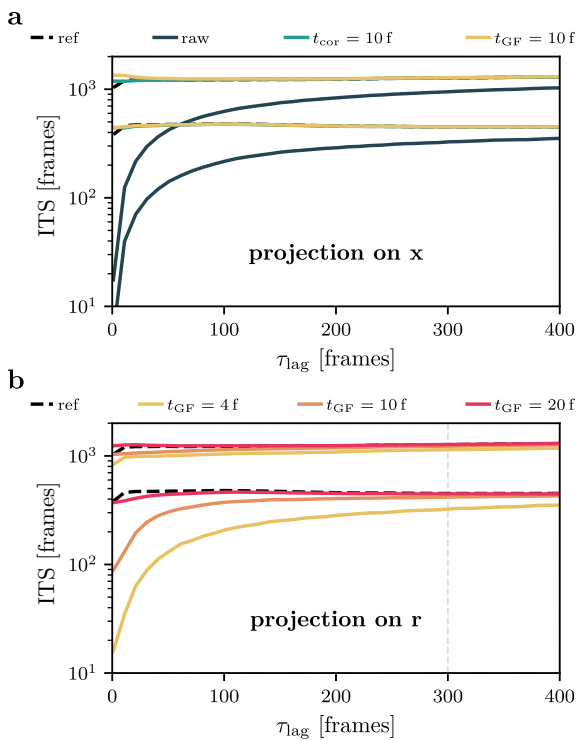


Figure 3: Implied timescales (ITSs) of the toy model, shown as a function of the lag time τ_{lag} . (a) Projecting on coordinate x , we show uncorrected data and results from iterative coring ($t_{\text{cor}} = 10$ frames, green) and Gaussian filtering ($t_{\text{GF}} = 10$ frames, yellow). (b) Projecting on coordinate r , we use Gaussian filtering ($t_{\text{GF}} = 4, 10, 20$ frames) to recover both ITSs. In all cases we compare to the reference timescales obtained for the optimal coordinate s (dashed black lines).

allows us to assign the filtered data to three states.

To construct a MSM from these data, we compute the transition probabilities between all states within some lag time τ_{lag} . Diagonalization of the resulting transition matrix yields the implied timescales (ITS) for each value of τ_{lag} , which can be used to assess how well an MSM reproduces the true dynamics of the system,⁵ see Fig. 3. For the full 2D model, as well as in the case of the optimal reaction coordinate s , we find Markovian behavior, with ITS independent of the lag time (black dashed lines). The slowest ITS t_1 reflects the main transition between states 1–2 and state 3, while the second t_2 captures the dynamics between state 1–3 and state 2.

Projecting on coordinate x , Fig. 3a compares the results obtained for raw data (black), with coring on the state trajectory (green), and with Gaussian filtering on x (yellow). While ITS obtained from the uncorrected data take a long lag time to converge to the reference results, both the coring and the Gaussian filtering results converge rapidly and reproduce the reference perfectly.

Projecting on coordinate r , uncorrected and cored data lead to a two-state model and therefore a single ITS. Although coring again improves this ITS, it cannot recover the third state. Gaussian filtering, on the other hand, is found to recover all three states for a filter window of $t_{\text{GF}} \gtrsim 4$ frames, and yields a constant second ITS for $t_{\text{GF}} = 20$ frames, see Fig. 3b.

Since both the coring time t_{cor} as well as the filtering window t_{GF} introduce a limit on the time resolution of the model, they need to be chosen shorter than the fastest timescale of interest. In particular, the lag time of an MSM built from cored and filtered data should be larger than t_{cor} and t_{GF} , respectively. To preserve a good time resolution of the model, we therefore want to choose t_{cor} and t_{GF} as short as possible, while still correcting the projection error. As a heuristic to choose the coring time t_{cor} , Nagel et al.²⁵ suggested to compute the probability $W_i(t)$ of staying in macrostate i for various coring times, and choose the shortest t_{cor} that suppresses the rapid initial decay reflecting spurious transitions at the barrier. As a consequence, this procedure yields improved and sufficiently converged ITSs. Accordingly, in the case of Gaussian filtering we want to determine the shortest filtering window t_{GF} that yields sufficiently converged ITSs and, in addition, the correct number of states.

We now study how the virtues of the above presented methods transfer to the treatment of high-dimensional MD data. To this end, we consider the folding of villin headpiece³⁶ (Fig. 4a), for which a 300 μs -long MD trajectory of the fast-folding Lys24Nle/Lys29Nle mutant (HP35) is publicly available from D. E. Shaw Research.³⁷ In a first step we determined the interresidue contacts of HP35, by assuming a contact to be formed if the distance d_{ij} between the closest non-hydrogen atoms of residues i and j

is shorter than 4.5 \AA , where $|i - j| > 3$ and d_{ij} is the minimal distance between all atom pairs of the two residues.^{29,38} To focus on native contacts, we request that contacts between these atoms pairs are populated for more than 30% of the simulation time,²⁹ which results in 42 native contacts. Using MoSAIC correlation analysis,³⁹ the associated contact distances are ordered in clusters of highly correlated contacts. Figure 4b shows the 27 contacts of the structurally most important clusters, which proceed along the protein backbone from the N- to the C-terminus. As a well-established 1D reaction coordinate,⁴⁰ we evaluated along the trajectory the fraction of native contacts formed, $Q(t)$, which nicely illustrates the time evolution of the folding process (Fig. 4c).

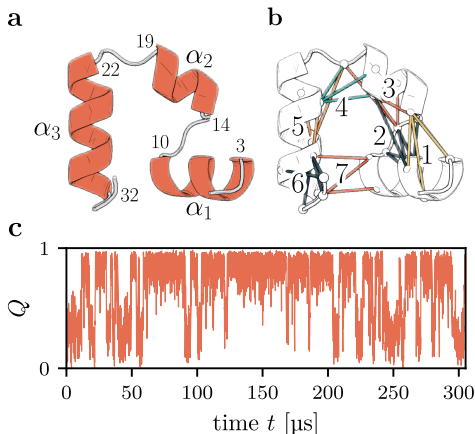


Figure 4: The folding of HP35. (a) Structure of the native state, and (b) illustration of the structurally most important 27 native contacts, ordered in seven MoSAIC clusters.³⁹ (c) Time evolution of the fraction of native contacts Q obtained from the folding trajectory by Piana et al.³⁷ Adapted from Ref. 29.

To obtain a simple estimate of the folding time, we define the unfolded region of the free energy landscape by $Q \lesssim 0.3$ and the native basin by $Q \gtrsim 0.7$, which allows us to directly count the folding events along the trajectory. Since $Q(t)$ exhibits fast fluctuations that do not necessarily account for a true folding or unfolding event, however, we need to invoke a procedure to eliminate this noise. As for the 2D model studied above, we can either require a minimum time to stay in the new region (i.e., dynamical coring), or apply a low-pass filter to

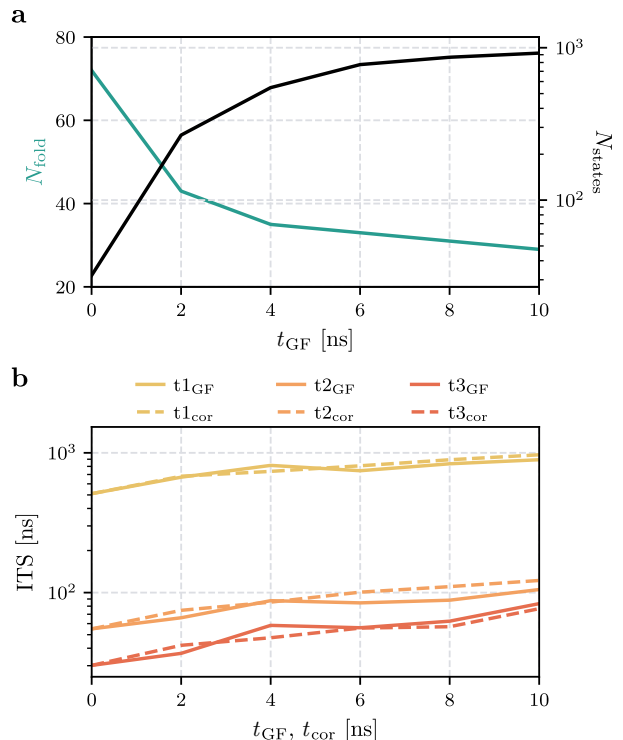


Figure 5: (a) Effects of Gaussian filtering with various filtering windows t_{GF} on the observed number of folding events N_{fold} of HP35 (green) and on the resulting number of microstates N_{states} obtained from robust density-based clustering¹⁸ (black). (b) First three implied timescales of MSMs obtained from coordinates filtered with different windows (full lines), and from dynamical coring on the microstates, using different coring times (dashed lines).

the data. In the following, we focus on the latter and employ Gaussian filtering of the contact distances used in the calculation of $Q(t)$.

Figure 5a shows the effects of Gaussian filtering on $Q(t)$, by depicting the number of folding events as a function of the filtering window t_{GF} applied to the contacts. While the uncorrected data overestimate the number of folding events by a factor 2, we find that it takes $t_{GF} \gtrsim 4 \text{ ns}$ to converge to about 30 folding events. This corresponds to a folding time of $\sim 2 \text{ } \mu\text{s}$, which is in agreement with previous works.³⁷ Yielding the correct folding time with minimal smoothing, $t_{GF} = 4 \text{ ns}$ was also chosen in the benchmark study by Nagel et al.²⁹

As discussed above, a major advantage of Gaussian filtering is that it can identify hidden conformational states, resulting in an im-

proved MSM. To explore this, we use the 42 native contact distances of HP35 as input coordinates in the subsequent analysis, and apply Gaussian filtering directly on these features. As dimensionality reduction step we use principal component analysis on the smoothed contact distances.⁴¹ The first five components exhibit a multimodal structure of their free energy curves, reveal the slowest timescales (~ 0.1 to $2 \mu\text{s}$), and explain $\sim 80\%$ of the total correlation.²⁹ Using these collective variables, we next perform robust density-based clustering.¹⁸ This clustering algorithm computes a local free energy estimate for every frame of the trajectory, by counting all other structures residing in a hypersphere of fixed radius. Reordering all structures by increasing free energy, the method directly yields the minima of the free energy landscape, where the number of these microstates depends on the chosen minimal population of a state (here $P_{\text{min}} = 0.01\%$). (This is unlike the popular k -means clustering, where this number needs to be specified beforehand.)

Using different windows t_{GF} to filter the contact distances, the above workflow yields clusterings with different number of microstates N_{states} . Remarkably, Fig. 5a shows that N_{states} increases drastically with t_{GF} , from 32 states for the uncorrected data ($t_{\text{GF}} = 0$), via 547 states ($t_{\text{GF}} = 4 \text{ ns}$) to 990 states ($t_{\text{GF}} = 10 \text{ ns}$), and stays approximately constant thereafter. This indicates that Gaussian filtering provides a significantly higher resolution of the underlying free energy landscape, confirming what we showed earlier for our toy model example.

To allow for a simple interpretation of an MSM, the numerous microstates are lumped into a few macrostates, which concisely account for the considered dynamical process. In this framework, differences between microstate partitionings do matter, because they may result in different macrostates and henceforth different dynamics. To group microstates into macrostates, we use the most probable path (MPP) algorithm,^{24,42} which constructs the transition matrix of the microstates and successively merges the state with the lowest metastability into the one to which it has the highest transition probability. Iteratively repeating this procedure yields a dendrogram that illus-

trates how the microstates aggregate into larger energy basins, which correspond to metastable conformational states. To resolve at least the first tier of the emerging hierarchical structure, we rely on the improved MPP algorithm²⁸ that ensures that the states have a minimum metastability of 0.5 and a minimum population of 0.5%, thus obtaining 12 metastable states. Showing these dendrograms for (a) uncorrected and (b,c) Gaussian-filtered data with $t_{\text{GF}} = 4 \text{ ns}$ and 10 ns , Fig. 6 clearly reveals the much larger number of microstates identified with Gaussian filtering. This leads to distinctly different lumping patterns and therefore also to different metastable states.

To illustrate this finding, Figs. 6d-f present structural characterizations of the three resulting macrostate partitionings. For each state, the distributions of contact distances in MoSAIC clusters 1–7 (Fig. 4b) are shown. The 12 macrostates are ordered by decreasing fractions of native contacts formed, such that state 1 corresponds to the native state (all distances shorter than 4.5 \AA), whereas state 12 represents the fully unfolded state, with a broad distribution of large distances.

We first discuss the Gaussian-filtered data with $t_{\text{GF}} = 4 \text{ ns}$ (panel e) as used in the benchmark study by Nagel et al.,²⁹ and are here referred to as ‘reference results’. The first three states are structurally well-defined, native-like conformations that differ mainly in the details of helix 1. States 4 and 5, which exhibit broken contacts near the C-terminus, still belong to the native energy basin. States 6–8 are sparsely populated ($\lesssim 1\%$) intermediates, while the unfolded basin comprises states 9–12, showing an increasing degree of structural disorder. In particular, we find a completely unfolded state 12 and two largely unfolded states 9 and 10 (with mainly intact contacts between helices α_2 and α_3 , see Fig. 4b), which renders transitions from state 12 to states 9 and 10 the most likely initial step of the folding process.²⁸

In contrast, the contact analysis of the uncorrected data (panel d) suggests that the first three states are merged into a single state. Obviously, the suppression of high-frequency fluctuations in the input data resulted in a better structural resolution of the native basin of

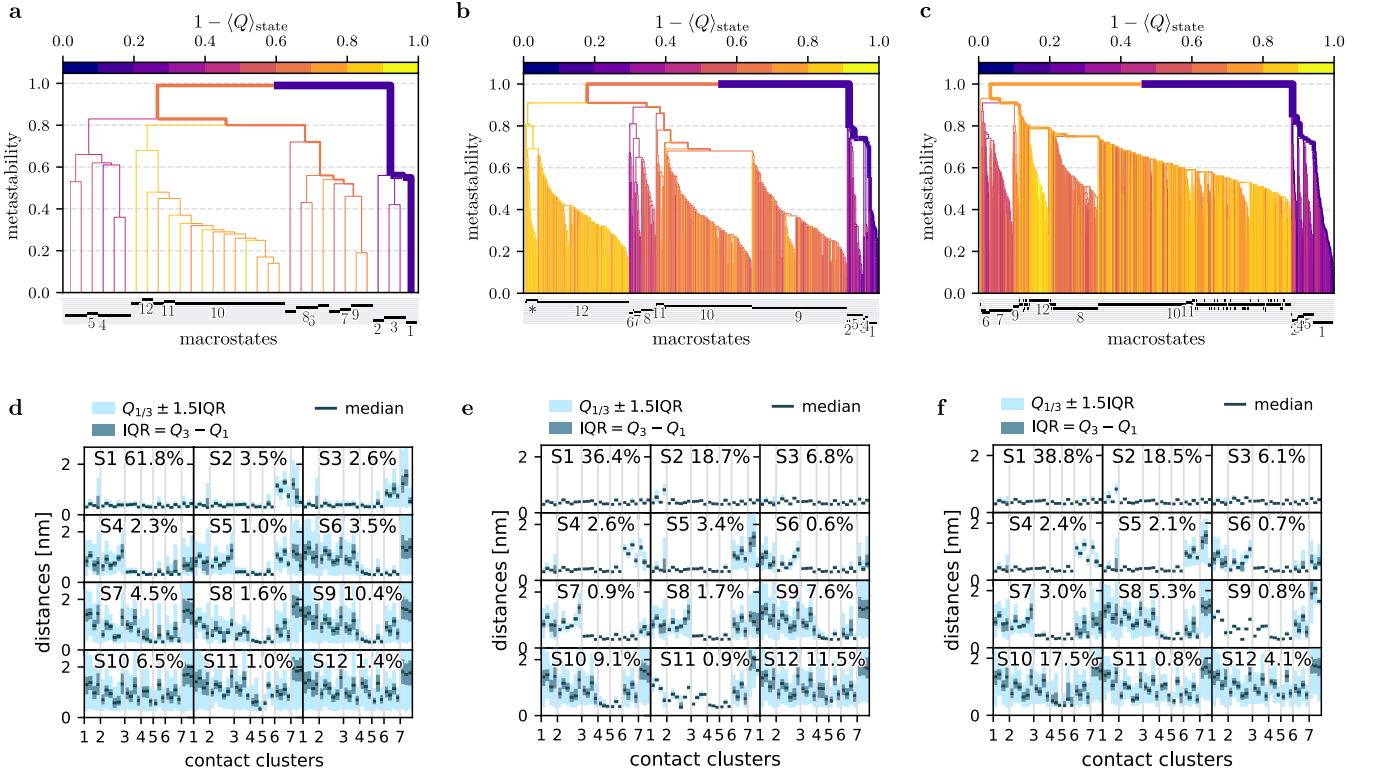


Figure 6: Construction of metastable conformational states describing the folding of HP35. Compared are uncorrected (a) data and Gaussian filtered data using (b) $t_{\text{GF}} = 4\text{ ns}$ and (c) $t_{\text{GF}} = 10\text{ ns}$. (Top) MPP dendrogram showing the hierarchical clustering of microstates into twelve metastable macrostates, using a lag time of 10 ns. Colors indicate the fraction of native contacts Q . (Bottom) Structural characterization of the resulting twelve metastable states of HP35, ordered by decreasing Q . For each state, the distribution of contact distances are represented by the median Q_2 , the interquartile range $\text{IQR} = Q_3 - Q_1$ and the lower (upper) bound as the smallest (largest) data point in $Q_{1/3} \pm 1.5 \cdot \text{IQR}$

HP35. Furthermore, the six states corresponding to the unfolded basin appear more congested and less distinctly separated than those obtained from the filtered reference data.

On the other hand, it is interesting to check if the state partitioning obtained for $t_{\text{GF}} = 10\text{ ns}$ (where the number of microstates is maximal) presents an improvement over the reference results with $t_{\text{GF}} = 4\text{ ns}$. While the first six states are virtually the same, we find that states 7 and 8 of the reference are lumped in one state, and that reference state 11 turns into state 9. The remaining unfolded states look similar to the reference state, but they do not clearly discriminate between the completely unfolded state and largely unfolded states with intact contacts between α_2 and α_3 .

Apart from the structural properties of the macrostates, it is important to assess the dy-

namics of the various MSMs. To this end, Fig. 5b shows their first three implied timescales (ITSs) as a function of the filtering window t_{GF} , assuming a lag time of 10 ns. We find a clear increase of the first ITS when comparing unfiltered ($t_{\text{GF}} = 0$) and reference ($t_{\text{GF}} = 4\text{ ns}$) results and a modest further improvement when using $t_{\text{GF}} = 10\text{ ns}$. Hence Gaussian filtering improves the Markovianity of the model, by increasing the energy barriers due to a higher resolution of the free energy landscape.

Following the discussion of the 2D model, we therefore conclude that $t_{\text{GF}} = 4\text{ ns}$ used in the benchmark study by Nagel et al.²⁹ represents a sweet spot of the filtering window range. As shown in Fig. 5, this choice yields good ITSs, the correct number of folding events N_{fold} , and a significantly increased number of microstates N_{states} . (Note that changing t_{GF} from 0 to 4 ns

results in an increase of N_{states} by $\sim 1600\%$, while changing to 5 ns only gives a further increase of $\sim 80\%$.) Resulting in a time resolution of $t_{\text{GF}} = 4$ ns, this minimal size of the filtering window still allows using relatively short lag times in the construction of the MSM.

We finally compare the above MSMs obtained using Gaussian filtering of the input coordinates to MSMs obtained using iterative dynamical coring of the microstates. To this end, Fig. 5b shows the first three ITSs as a function of the coring time t_{cor} . Recalling that we need to choose $t_{\text{cor}} \approx t_{\text{GF}}$ to achieve a similar time resolution, we find that coring and filtering yield virtually the same timescales. However, as coring is applied to the microstates, it cannot achieve the improved structural resolution of the free energy landscape found for filtering (see Fig. 6). In fact, the structural characterization of the macrostates obtained from coring (with $t_{\text{cor}} = 4$ ns) is virtually identical to the results obtained without coring shown in Fig. 6d. In other words, dynamical coring only improves the dynamics of the resulting MSM, while Gaussian filtering improves in addition the structural properties of the macrostates of the model. Due to the complementary nature of the two methods, it may nevertheless be advantageous to use both corrections in order to optimize the Markovianity of the model.

In conclusion, we have shown that Gaussian filtering of input coordinates can significantly improve the performance of an MSM. Apart from naturally improving the timescale separation and therefore the implied timescales of the model, the reduction of the fluctuations may greatly facilitate the identification of microstates in the subsequent clustering of the data. We emphasize that this improved representation of the free energy landscape is only achieved because the filtering is applied at the very beginning of the trajectory analysis. In contrast, related approaches that correct for projection artifacts—such as dynamical coring of the state trajectory—cannot provide the same benefit. As the method is fully compatible with any subsequent workflow used to construct an MSM, we propose that initial Gaussian filtering of the feature trajectory should become a standard component of the MSM workflow.

Acknowledgments

This work has been supported by the Deutsche Forschungsgemeinschaft (DFG) within the framework of the Research Unit FOR 5099 “Reducing complexity of nonequilibrium” (project No. 431945604), the High Performance and Cloud Computing Group at the Zentrum für Datenverarbeitung of the University of Tübingen and the Rechenzentrum of the University of Freiburg, the state of Baden-Württemberg through bwHPC and the DFG through grant no INST 37/935-1 FUGG (RV bw16I016), and the Black Forest Grid Initiative.

Data Availability Statement

The simulation data and all intermediate results for our reference model of HP35, including our software packages *MoSAIC*,³⁹ *Fast-PCA*,⁴³ *Clustering*¹⁸ and *msmhelper*¹⁰ and detailed descriptions to reproduce all steps of the workflow, can be downloaded from <https://github.com/moldyn/HP35>.

References

- (1) Berendsen, H. J. *Simulating the Physical World: Hierarchical Modeling from Quantum Mechanics to Fluid Dynamics*; Cambridge University Press, 2007.
- (2) Chodera, J. D.; Swope, W. C.; Pitner, J. W.; Dill, K. A. Obtaining long-time protein folding dynamics from short-time molecular dynamics simulations. *Multi-scale Modeling & Simulation* **2006**, *5*, 1214–1226.
- (3) Buchete, N.-V.; Hummer, G. Coarse master equations for peptide folding dynamics. *J. Phys. Chem. B* **2008**, *112*, 6057–6069.
- (4) Bowman, G. R.; Beauchamp, K. A.; Boxer, G.; Pande, V. S. Progress and challenges in the automated construction of Markov state models for full protein systems. *J. Chem. Phys.* **2009**, *131*, 124101, Publisher: AIP.

- (5) Prinz, J.-H.; Wu, H.; Sarich, M.; Keller, B.; Senne, M.; Held, M.; Chodera, J. D.; Schütte, C. et al. Markov models of molecular kinetics: generation and validation. *J. Chem. Phys.* **2011**, *134*, 174105.
- (6) Bowman, G. R., Pande, V. S., Noé, F., Eds. *An introduction to Markov state models and their application to long timescale molecular simulation*; Advances in experimental medicine and biology 797; Springer, 2014.
- (7) Wang, W.; Cao, S.; Zhu, L.; Huang, X. Constructing Markov State Models to elucidate the functional conformational changes of complex biomolecules. *WIREs Comp. Mol. Sci.* **2018**, *8*, e1343.
- (8) Scherer, M. K.; Trendelkamp-Schroer, B.; Paul, F.; Perez-Hernandez, G.; Hoffmann, M.; Plattner, N.; Wehmeyer, C.; Prinz, J.-H. et al. PyEMMA 2: A Software Package for Estimation, Validation, and Analysis of Markov Models. *J. Chem. Theory Comput.* **2015**, *11*, 5525–5542.
- (9) Beauchamp, K. A.; Bowman, G. R.; Lane, T. J.; Maibaum, L.; Haque, I. S.; Pande, V. S. MSMBuilder2: Modeling Conformational Dynamics on the Picosecond to Millisecond Scale. *J. Chem. Theory Comput.* **2011**, *7*, 3412–3419.
- (10) Nagel, D.; Stock, G. msmhelper: A Python package for Markov state modeling of protein dynamics. *J. Open Source Softw.* **2023**, *8*, 5339.
- (11) Hegger, R.; Altis, A.; Nguyen, P. H.; Stock, G. How Complex is the Dynamics of Peptide Folding? *Phys. Rev. Lett.* **2007**, *98*, 028102.
- (12) Facco, E.; d’Errico, M.; Rodriguez, A.; Laio, A. Estimating the intrinsic dimension of datasets by a minimal neighborhood information. *Sci. Rep.* **2017**, *7*, 12140.
- (13) Amadei, A.; Linssen, A. B. M.; Berendsen, H. J. C. Essential dynamics of proteins. *Proteins* **1993**, *17*, 412–425.
- (14) Wang, Y.; Ribeiro, J. M. L.; Tiwary, P. Machine learning approaches for analyzing and enhancing molecular dynamics simulations. *Curr. Opin. Struct. Biol.* **2020**, *61*, 139–145.
- (15) Glielmo, A.; Husic, B. E.; Rodriguez, A.; Clementi, C.; Noé, F.; Laio, A. Unsupervised Learning Methods for Molecular Simulation Data. *Chem. Rev.* **2021**, *121*, 9722–9758.
- (16) Keller, B.; Daura, X.; Gunsteren, W. F. v. Comparing geometric and kinetic cluster algorithms for molecular simulation data. *J. Chem. Phys.* **2010**, *132*, 074110.
- (17) Rodriguez, A.; Laio, A. Clustering by fast search and find of density peaks. *Science* **2014**, *344*, 1492–1496, Publisher: American Association for the Advancement of Science.
- (18) Sittel, F.; Stock, G. Robust Density-Based Clustering to Identify Metastable Conformational States of Proteins. *J. Chem. Theory Comput.* **2016**, *12*, 2426–2435.
- (19) Song, L.; Lizhe, Z.; Kit, S. F.; Wei, W.; Huang, X. Adaptive partitioning by local density-peaks: An efficient density-based clustering algorithm for analyzing molecular dynamics trajectories. *J. Comput. Chem.* **2017**, *38*, 152–160.
- (20) Jain, A. K. Data clustering: 50 years beyond K-means. *Pattern Recognit. Lett.* **2010**, *31*, 651 – 666.
- (21) Sittel, F.; Stock, G. Perspective: Identification of Collective Coordinates and Metastable States of Protein Dynamics. *J. Chem. Phys.* **2018**, *149*, 150901.
- (22) Schütte, C.; Noé, F.; Lu, J.; Sarich, M.; Vanden-Eijnden, E. Markov state models based on milestoning. *J. Chem. Phys.* **2011**, *134*, 204105, Publisher: AIP.

- (23) Lemke, O.; Keller, B. G. Density-based cluster algorithms for the identification of core sets. *J. Chem. Phys.* **2016**, *145*, 164104.
- (24) Jain, A.; Stock, G. Hierarchical folding free energy landscape of HP35 revealed by most probable path clustering. *J. Phys. Chem. B* **2014**, *118*, 7750 – 7760.
- (25) Nagel, D.; Weber, A.; Lickert, B.; Stock, G. Dynamical coring of Markov state models. *J. Chem. Phys.* **2019**, *150*, 094111.
- (26) Wang, D.; Wang, Y.; Evans, L.; Tiwary, P. From Latent Dynamics to Meaningful Representations. *J. Chem. Theory Comput.* **2024**, *20*, 3503–3513, Publisher: American Chemical Society.
- (27) Diez, G.; Dethloff, N.; Stock, G. Recovering hidden degrees of freedom using Gaussian processes. *J. Chem. Phys.* **2025**, *163*, 124105.
- (28) Nagel, D.; Sartore, S.; Stock, G. Selecting Features for Markov Modeling: A Case Study on HP35. *J. Chem. Theory Comput.* **2023**, *19*, 3391 – 3405.
- (29) Nagel, D.; Sartore, S.; Stock, G. Toward a Benchmark for Markov State Models: The Folding of HP35. *J. Phys. Chem. Lett.* **2023**, *14*, 6956–6967.
- (30) Deng, G.; Cahill, L. An adaptive Gaussian filter for noise reduction and edge detection. 1993 IEEE Conference Record Nuclear Science Symposium and Medical Imaging Conference. 1993; pp 1615–1619 vol.3.
- (31) Jaipal, M.; Chatterjee, A. Relative Occurrence of Oxygen-Vacancy Pairs in Yttrium-Containing Environments of Y2O3-Doped ZrO2 Can Be Crucial to Ionic Conductivity. *J. Phys. Chem. C* **2017**, *121*, 14534–14543.
- (32) Tan, Z. W.; Guarnera, E.; Berezhovsky, I. N. Exploring chromatin hierarchical organization via Markov State Modelling. *PLOS Comp. Bio.* **2018**, *14*, e1006686.
- (33) Krivov, S. V. On Reaction Coordinate Optimality. *J. Chem. Theory Comput.* **2013**, *9*, 135–146.
- (34) Diez, G. Markov Modeling of Nonequilibrium Biomolecular Data. M.Sc. thesis, University of Freiburg, Germany, 2020.
- (35) The improvement is modest for the simple 2D model: for $t_{\text{cor}} = 10$ frames standard and iterative coring reassign 5.14% vs. 5.33% of the MD frames, respectively; for $t_{\text{cor}} = 50$ frames, though, we already find 5.29% vs. 13.95%. For a complex system such as HP35 considered below the effect is more substantial already at short coring times, e.g., we obtain 7.79% vs. 11.57% for $t_{\text{cor}} = 2$ ns, and 8.98% vs. 15.03% for $t_{\text{cor}} = 4$ ns.
- (36) Kubelka, J.; Henry, E. R.; Cellmer, T.; Hofrichter, J.; Eaton, W. A. Chemical, physical, and theoretical kinetics of an ultrafast folding protein. *Proc. Natl. Acad. Sci. USA* **2008**, *105*, 18655–18662.
- (37) Piana, S.; Lindorff-Larsen, K.; Shaw, D. E. Protein folding kinetics and thermodynamics from atomistic simulation. *Proc. Natl. Acad. Sci. USA* **2012**, *109*, 17845–17850.
- (38) Yao, X.-Q.; Momin, M.; Hamelberg, D. Establishing a Framework of Using Residue–Residue Interactions in Protein Difference Network Analysis. *J. Chem. Inf. Model.* **2019**, *59*, 3222–3228.
- (39) Diez, G.; Nagel, D.; Stock, G. Correlation-based feature selection to identify functional dynamics in proteins. *J. Chem. Theory Comput.* **2022**, *18*, 5079 – 5088.
- (40) Best, R. B.; Hummer, G.; Eaton, W. A. Native contacts determine protein folding mechanisms in atomistic simulations. *Proc. Natl. Acad. Sci. USA* **2013**, *110*, 17874–17879.

- (41) Ernst, M.; Sittel, F.; Stock, G. Contact- and distance-based principal component analysis of protein dynamics. *J. Chem. Phys.* **2015**, *143*, 244114.
- (42) Jain, A.; Stock, G. Identifying metastable states of folding proteins. *J. Chem. Theory Comput.* **2012**, *8*, 3810 – 3819.
- (43) Sittel, F.; Filk, T.; Stock, G. Principal component analysis on a torus: Theory and application to protein dynamics. *J. Chem. Phys.* **2017**, *147*, 244101.